CHALMERS
UNIVERSITY OF TECHNOLOGY

Modeling of laminated veneer lumber

A study of the material properties for thick structural elements

Master's thesis in Applied Mechanics and Structural Engineering and Building Technology

JOHN EK
VIKTOR NORBÄCK

Department of Architecture and Civil Engineering
CHALMERS UNIVERSITY OF TECHNOLOGY
Göteborg, Sweden 2020

MASTER'S THESIS IN APPLIED MECHANICS AND STRUCTURAL ENGINEERING AND BUILDING TECHNOLOGY

Modeling of laminated veneer lumber

A study of the material properties for thick structural elements

JOHN EK
VIKTOR NORBÄCK

Department of Architecture and Civil Engineering
Division of Structural Engineering
CHALMERS UNIVERSITY OF TECHNOLOGY
Göteborg, Sweden 2020

Modeling of laminated veneer lumber - A study of the material properties for thick structural elements
JOHN EK
VIKTOR NORBÄCK

Department of Architecture and Civil Engineering
Division of Structural Engineering
Chalmers University of Technology
SE-412 96 Göteborg
Sweden
Telephone: +46 (0)31-772 1000

Modeling of laminated veneer lumber - A study of the material properties for thick structural elements
Master's thesis in Applied Mechanics and Structural Engineering and Building Technology
JOHN EK, VIKTOR NORBÄCK
Department of Architecture and Civil Engineering
Division of Structural Engineering
Chalmers University of Technology

Abstract

This thesis studies the material properties of laminated veneer lumber (LVL). LVL is a timber product made of thin veneers of wood, glued together to form a laminate. The work has been carried out with the aim of providing a better understanding of LVL when designing large structures, in particular the thesis is related to the large scale application of wind turbine towers.

The project consists of two major parts, initially a study of the possibility to use laminate theory for evaluation of LVL stiffness parameters. From this study it was found that the laminate theory used, in combination with the accessible material parameters provide an unfit description of the material. Consequently the second part of the project investigates the material behaviour using a more advanced three dimensional model, taking the effect of variability in veneer properties and the influence of knots, modeled as stiffness free voids, into account. The study reveal that increasing the number of veneers, increases the effect from the variability of veneers and reduces the influence of knots.

Conclusions from the model suggests there are both beneficial and unfavourable effects when designing thick LVL structures. In order to account for these effects which currently is not practice, a more elaborate three dimensional model need to be studied, analyzing the material further.

Keywords: Laminated veneer lumber (LVL), Laminate theory, Finite elements

Preface

The thesis was carried out at Chalmers University of Technology in collaboration with the engineering company Modvion, during the spring of 2020.

We thank our supervisors Robert Jockwer and Rasoul Atashipour for the discussions and guidance throughout the project. We also thank Fredrik Larsson for his valuable support on finite element modeling.

Lastly we thank Modvion, for the much appreciated study visit at the factory in Töreboda and Geir Söderin for his assistance.

John Ek and Viktor Norbäck, Gothenburg, 2020

Contents

1 Introduction

A Swedish engineering company Modvion is developing large scale structures made from laminated wood, specifically Laminated Veneer Lumber (LVL). These applications require the material to be used close to its structural limit, which compels proper understanding of the material properties. The current potential sources of these properties are either data from smaller prefabricated products or from tests performed on the components. The prefabricated products differ from the components used in Modvion's structures and thus can not fully capture the properties of the wind turbine tower. Furthermore, testing of the full scale components brings high cost in terms of both time and resources.

A material model capable of predicting the strength and stiffness of LVL in these large scale applications is thus desired to be able to capture the structural behaviour and make testing more efficient. The particular structure developed by Modvion relating to this project is the design of 150 m high wind turbine towers. A conceptual image of a tower and the assembly can be seen in Figure 1.1.

Figure 1.1: Assembly of turbine towers [1].

The towers are assembled from modules, made of eight to ten LVL sheets, each sheet is 27 mm thick and consists of nine cross-bonded softwood veneers. Three to eight modules are assembled to form a tubular section and the sections are stacked to form the tower. Pictures of various modules and sections used by Modvion can be seen in Figure 1.2.

a Example module.

b Modules used for prototype tower.

c Assembled sections of the prototype tower.

Figure 1.2: Modules and sections used by Modvion [1].

The modules are produced by lamination of the LVL sheets, which are curved to the shape of the sections. The essential steps of the module production are shown in Figure 1.3.

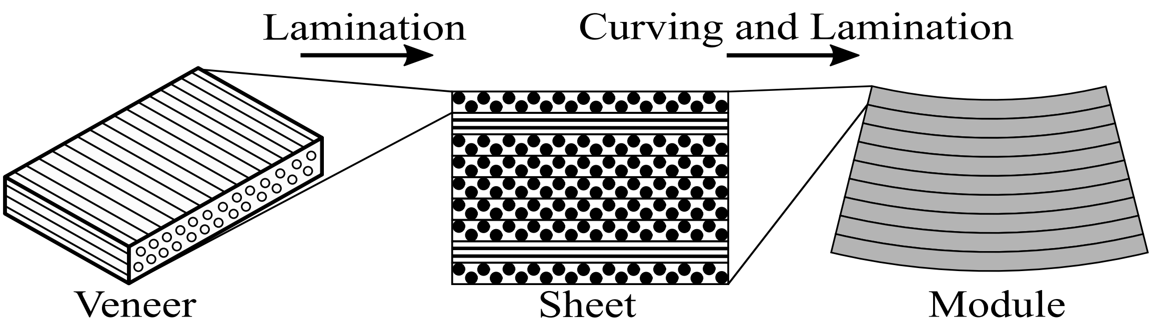

Figure 1.3: Production of modules with example layup.

Modvion advocates several benefits to this way of building wind turbine towers; the modules are light, small in size and assembled to cylinders on site, meaning that transportation can be simplified and made more efficient compared to conventional steel towers [1], which are transported as larger cylindrical parts to the building site. Furthermore, the production of timber requires significantly less energy and emissions in relation to steel [2]. The combined effect of improved transportation, beneficial production and the use of timber, which is a less energy demanding, renewable material, results in a more sustainable product.

1.1 Project aim

In order to improve the structural performance of the wind turbine tower, accurate methods to determine the strength is desired. This work investigates the possibility of using laminate theory to predict the material behaviour. In addition, the effect of knots and variability of stiffness in individual veneers is studied for very thick LVL.

1.2 Method

From the material data of tested standardized LVL products, laminate theory is used to evaluate the stiffness properties of a single veneer. Veneer properties from standardized products as well as raw material data are used to evaluate the properties of laminates with an arbitrary layup and thickness.

A 3D finite element (FE) model is developed where defects and variability of stiffness of veneers are included. Through Monte Carlo simulation, i.e. simulating many models containing different statistically determined deviations in the material, the effect of size for thick LVL cross sections is investigated. The Monte Carlo simulations are performed and compared for four different laminates of varying size, each with a unidirectional tensile load.

1.3 Limitations

For both the laminate theory and the 3D model, the following limitations apply:

- Full interaction between laminates is assumed. Delamination and stiffness variation in the interface between veneers is not accounted for in the models.
- The models make no distinction between lamination of veneers and the lamination of sheets. In reality the lamination of veneers to sheets will possess different properties than the lamination of sheets to produce modules.
- The fibers are modeled perfectly aligned with the veneer edges.
- The tower is cylindrical, using curved laminates as walls. The curvature of the LVL is not included in this study.

The Monte Carlo simulations are performed with the additional simplifications and demarcations:

- The 3D material model is linear elastic, meaning it is unable to predict plastic redistribution of stresses. The project focuses on the load paths due to discontinuities in the material and not predicting the actual strength of the material.
- Only the load case with uniaxial tensile stress is modeled in the 3D FE-model. Bending, shear and compression is not studied in this work.
- In the 3D model defects are considered as cuboid voids of equal size. In reality the knots vary in shape and size and may provide some stiffness to the material.
- The Monte Carlo simulation is made for ten thousand runs. This work focuses on observing a trend and ten thousand are considered sufficient for this intent.

2 Problem description

Engineered wood products (EWP) are designed timber products where the mechanical properties of the raw timber material is improved through various production methods [3]. LVL is an EWP made from thin veneers of wood, glued together to form a laminate [4]. There are several benefits of gluing veneers together compared to structural timber. Decreased variability in material properties, the shape not being limited by the raw material and the possibility to have more than one fiber direction within the same product are some of the benefits. The LVL sheets used by Modvion are laminated using a water and boiling proof (WBP) phenolic adhesive and veneers made from Nordic spruce [5].

2.1 Production

Production of LVL starts from timber logs being debarked and conditioned in a condition chamber, resulting in bark free soft logs. The logs are cut into pieces and mounted on a rotation peeler where a peeling lathe peels the log into veneers [4]. Figure 2.1 illustrates the peeling of a log and the longitudinal- (L), radial- (R) and transverse/tangential (T) directions i relation to the fibers.

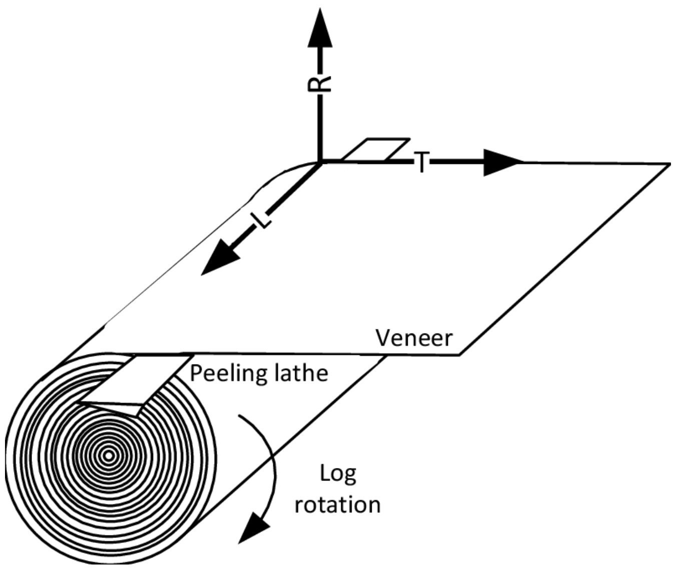

Figure 2.1: Sketch of veneer peeling from a log [6].

The organic nature of timber add a variability to its properties [7]. In addition, the quality of the material is different depending on its distance from the centre of the peeling billet, where the strongest material is located at the edge [4]. This means the stiffness and strength properties change depending on where through the thickness, the veneer was peeled. Both these effects imply a variability of veneer properties within the LVL product. The veneers are then glued- and hot pressed together, forming the final LVL product. The resulting interface between each veneer consists of a material that is a mixture between wood fibers and glue [8]. Furthermore, the bond between veneers and sheets generally possess higher strength and stiffness than the individual veneers [9].

Due to the peeling of logs, the presence of knots will be distributed with a repeating pattern in the veneers. As the peeling lathe cuts through a single knot multiple times, this results in strips of cut knots in the veneers, with a distance relating to the diameter of the wood billet. Modeling of knot distribution in the veneers is further described in Section 4.5.

2.2 standardized products

LVL typically refer to laminated wood products with a dominating part of the veneers oriented in the same direction. Examples of standardized LVL products are Kerto-S and Kerto-Q. Kerto-S consist only of longitudinal veneers typically used for beams. Kerto-Q consists of additional veneers in the transversal direction, located in the vicinity of the laminate edges and is typically used for plates [4]. This is a distinction between other laminated wood products such as plywood, which typically uses a cross-ply lamination, meaning that longitudinal and transversal veneers are alternated throughout the laminate. Examples of Kerto-S and Kerto-Q products provided by LVL producer Metsä Wood are seen in Figure 2.2.

a Kerto-S, beams with only longitudinal veneers.

b Kerto-Q, panels with longitudinal and transversal veneers.

Figure 2.2: LVL products, Metsä Wood [10].

Kerto-S, Kerto-Q and plywood are made of symmetric layups, meaning they are mirrored over the mid-plane of the thickness. In general both Kerto-Q and plywood products consist of only longitudinal and transversal veneers. The standardized products do not offer the dimensions required for the application of wind turbine towers and therefore the modules used by Modvion do not consist of standardized sheets. However, the demarcation to only longitudinal and transversal veneers as well as the type of timber and adhesive used correspond to standardized Kerto-Q. Therefore the material properties of Kerto-Q will be used as a basis when predicting the properties of the wind turbine tower.

2.3 Veneer effect

As mentioned in Section 2.1 the production of LVL will give a variability of the individual veneers in a laminate. This will have an impact on the stress distribution in the cross section where regions with higher stiffness will attract more load compared to regions with lower stiffness. Consequently high stiffness veneers in proximity to low stiffness veneers can induce a stress concentration in the stiffer veneer. Depending on the size of the cross section, i.e. the number of veneers, this can have varying impact. The influence of the variation in veneer properties for laminates of varying thickness will be referred to as veneer effect.

2.4 Size effect

When predicting the behaviour of timber one must consider defects embedded in the material, such defects are weak spots that will determine its strength [11]. The impact of defects is a probabilistic phenomena depending on the size of the timber structure, mainly occurring in the tensile zone of a loaded body [11]. This phenomena is known as the size effect and implicates that larger volumes of timber are more likely to include defects than smaller volumes [12]. In design according to Eurocode 5[1], sufficiently small members of structural timber and EWP, such as glued laminated timber (Glulam) and LVL may have their characteristic strength increased due to a lower probability of defects [13].

In Modvion's application for the wind turbine towers, the wall cylinder will be 216-270 mm thick, which is thicker than the average structural member made of timber. For large structural members there is no modification of the characteristic strength in Eurocode 5 [13].

2.5 Homogenization

The geometry of a knot is close to the shape of a cone [14]. In addition the fibers in timber are not perfectly aligned, there are deviations due to timber's organic nature. Furthermore there are local larger angle deviations in the fibers around knots [15].

From the peeling process in the production of LVL, the cone shaped knots are cut into smaller defects distributed over the volume of the laminate [4], meaning that the maximum thickness of a knot defect equals the thickness of a single veneer. For a given type of veneer, the size of a defect is independent of the thickness of the laminate. Therefore the volume of a single knot relative to the total volume of the laminate is lower for thicker laminates and the impact of knots can vary depending on the thickness of laminates. This will be referred to as homogenization, not to be confused with the size effect described in Eurocode 5 [13]. It is expected that for a thick construction with a lot of veneers e.g. the wind turbine tower built by Modvion, homogenization will have a larger impact and thus lower the influence of defects in the material.

[1]European standard for design of timber structures

3 Evaluation of stiffness properties

Due to the combined effect of timber's organic nature and the laminate structure, complex material models are required to describe the mechanical properties of LVL in detail. A simplified method is investigated, utilizing laminate theory, which is a theoretical tool used to analyse the mechanical behaviour of composite materials. Laminate theory is commonly used for fiber-reinforced polymers and has the benefit that it constitute several simplifications to the complex three dimensional problem.

The theory assembles and evaluates the properties and mechanical response for laminates consisting of plies (veneers in timber products) with different fiber directions. Plies are the components by which a laminate is composed, in laminate theory a ply is considered as a plate element with a uniform fiber direction. Composite mechanics and laminate theory are described in a similar way in a variety of literature. Assumptions, equations and the notation used in this report can be found in both [16, 17]. A significant assumption in laminate theory is that the fibers are assumed perfectly aligned within each ply. In addition the laminate theory used in this report assumes the bonding between plies to be ideal, i.e. no deformations due to shear can occur between the layers. This is not common practice for all types of laminate theory.

3.1 Laminate orientation

In order to describe the layup of veneers in a laminate, this report will use a notation based on the Cartesian coordinate system, where the coordinates are defined using the fiber direction of the majority of the veneers as the global x-direction. The y-axis is the in-plane direction perpendicular to the x-axis and the z-axis is the out-of-plane direction. The notation assumes equally thick plies and same ply properties throughout the laminate. Figure 3.1 show an example cross section of a five veneer laminate and the coordinate axis.

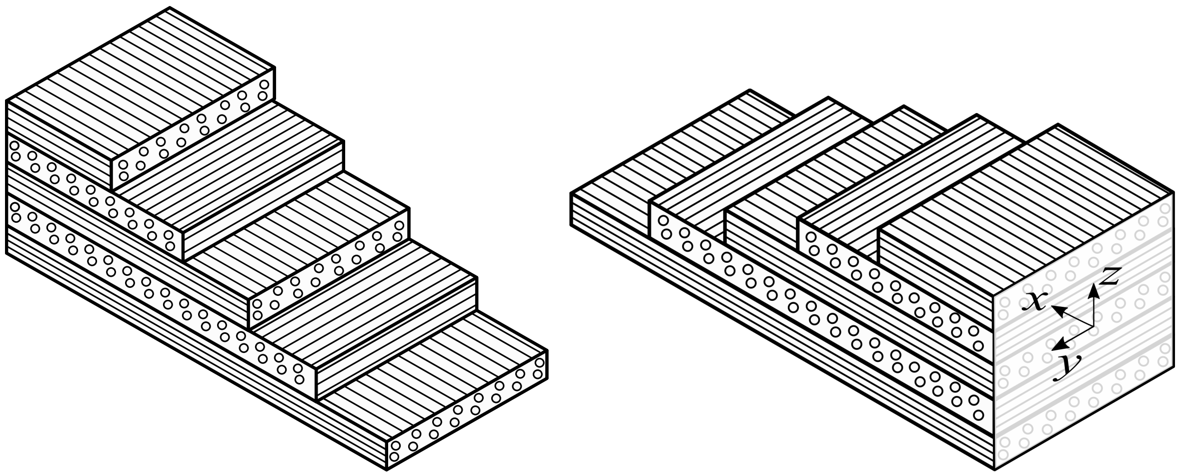

Figure 3.1: Sketch of a five veneer laminate with global coordinate system.

In the chosen laminate notation the layup above is described with the following expression

$$\text{Layup} = [0/90/\bar{0}]_\text{s} \tag{3.1}$$

the inherent numbers are the fiber direction in degrees from the global x-axis for each individual veneer. Since the layup is symmetric, only the veneers up to the symmetry line is written, where the subscript s indicates symmetry of the entire laminate. In cases of symmetry with odd number of veneers the symmetry line splits the center veneer, such veneers are denoted with a bar as seen in Eq. (3.1).

3.2 Laminate theory

Laminate theory originate from the generalized Hooke's law for a linear elastic material. By utilizing the symmetry of the Cauchy stress- and strain tensors $\boldsymbol{\sigma}$ and $\boldsymbol{\varepsilon}$ (minor symmetry of the fourth-order Hooke elasticity tensor C), the constitutive relation can be written in contracted matrix or Voigt format as

$$\begin{bmatrix} \sigma_1 \\ \sigma_2 \\ \sigma_3 \\ \sigma_{23} \\ \sigma_{13} \\ \sigma_{12} \end{bmatrix} = \begin{bmatrix} C_{11} & C_{12} & C_{13} & C_{14} & C_{15} & C_{16} \\ C_{21} & C_{22} & C_{23} & C_{24} & C_{25} & C_{26} \\ C_{31} & C_{32} & C_{33} & C_{34} & C_{35} & C_{36} \\ C_{41} & C_{42} & C_{43} & C_{44} & C_{45} & C_{46} \\ C_{51} & C_{52} & C_{53} & C_{54} & C_{55} & C_{56} \\ C_{61} & C_{62} & C_{63} & C_{64} & C_{65} & C_{66} \end{bmatrix} \begin{bmatrix} \varepsilon_1 \\ \varepsilon_2 \\ \varepsilon_3 \\ \gamma_{23} \\ \gamma_{13} \\ \gamma_{12} \end{bmatrix} \tag{3.2}$$

where the indices 1, 2 and 3 correspond to x, y and z components of the stress and strain. Eq. (3.2) is written in the condensed format as

$$\underline{\boldsymbol{\sigma}} = \underline{\boldsymbol{C}}\,\underline{\boldsymbol{\varepsilon}} \tag{3.3}$$

where $\underline{\boldsymbol{C}}$ is the matrix representation of the fourth-order Hooke tensor C. Restricting to the small strain setting (Cauchy stress) entails that the Hooke tensor acquire major symmetry, further reducing the tensor to 21 individual components. In addition laminate theory consider laminates as a specially orthotropic material, meaning that they fulfill symmetry conditions in the xy- and xz-plane. Major symmetry of the Hooke tensor along with the properties of a specially orthotropic material, reduces the constitutive matrix to

$$\underline{\boldsymbol{C}} = \begin{bmatrix} C_{11} & C_{12} & C_{13} & 0 & 0 & 0 \\ C_{12} & C_{22} & C_{23} & 0 & 0 & 0 \\ C_{13} & C_{23} & C_{33} & 0 & 0 & 0 \\ 0 & 0 & 0 & C_{44} & 0 & 0 \\ 0 & 0 & 0 & 0 & C_{55} & 0 \\ 0 & 0 & 0 & 0 & 0 & C_{66} \end{bmatrix} \tag{3.4}$$

Evaluation of laminates are in general based on the assumption that the axial out-of-plane component, σ_3, is set to 0, due to their planar dimensions (small height relative to the depth and length). This means that a laminate can be fully described by six individual components; C_{11}, C_{12}, C_{22}, C_{44}, C_{55} and C_{66}. Each component can be expressed in their fibre- or sub-scale components as

$$C_{11} = \frac{E_L}{1-\nu_{LT}\nu_{TL}}, \qquad C_{12} = \frac{\nu_{TL}E_L}{1-\nu_{LT}\nu_{TL}}, \qquad C_{22} = \frac{E_T}{1-\nu_{LT}\nu_{TL}} \tag{3.5}$$

$$C_{44} = G_{RT}, \qquad C_{55} = G_{LR}, \qquad C_{66} = G_{LT} \tag{3.6}$$

where the indices L, R and T represent the longitudinal-, radial- and transverse/tangential directions in relation to the wood fibers, corresponding to Figure 2.1. ν_{ij} and ν_{ji} are the major and minor Poisson's ratios, where it is noted from the symmetry of $\underline{\boldsymbol{C}}$ that

$$\nu_{ij}E_j = \nu_{ji}E_i \tag{3.7}$$

The constitutive matrix is commonly split into two separate parts by defining the in-plane stiffness as

$$\hat{\underline{\boldsymbol{C}}} = \begin{bmatrix} C_{11} & C_{12} & 0 \\ C_{21} & C_{22} & 0 \\ 0 & 0 & C_{66} \end{bmatrix} = \begin{bmatrix} \dfrac{E_L}{1-\nu_{LT}\nu_{TL}} & \dfrac{\nu_{TL}E_L}{1-\nu_{LT}\nu_{TL}} & 0 \\ \dfrac{\nu_{TL}E_L}{1-\nu_{LT}\nu_{TL}} & \dfrac{E_T}{1-\nu_{LT}\nu_{TL}} & 0 \\ 0 & 0 & G_{LT} \end{bmatrix} \tag{3.8}$$

and the corresponding out-of-plane stiffness as

$$\underline{\tilde{\boldsymbol{C}}} = \begin{bmatrix} C_{44} & 0 \\ 0 & C_{55} \end{bmatrix} = \begin{bmatrix} G_{RT} & 0 \\ 0 & G_{LR} \end{bmatrix} \tag{3.9}$$

where $\underline{\hat{\boldsymbol{C}}}$ and $\underline{\tilde{\boldsymbol{C}}}$ represent the *local* stiffness matrices for each ply.

The in-plane mechanical properties for the laminate are described using the assembled stiffnesses $\underline{\boldsymbol{A}}$, $\underline{\boldsymbol{B}}$ and $\underline{\boldsymbol{D}}$ known as the extensional, coupling and bending matrices. The matrices are evaluated using the assembly procedure as

$$\underline{\boldsymbol{A}} = \sum_{k=1}^{N} \overline{\underline{\hat{\boldsymbol{C}}}}_k (h_k - h_{k-1}), \qquad \underline{\boldsymbol{B}} = \sum_{k=1}^{N} \overline{\underline{\hat{\boldsymbol{C}}}}_k (h_k^2 - h_{k-1}^2), \qquad \underline{\boldsymbol{D}} = \sum_{k=1}^{N} \overline{\underline{\hat{\boldsymbol{C}}}}_k (h_k^3 - h_{k-1}^3) \tag{3.10}$$

where N are the number of plies, h_k and h_{k-1} are the z-coordinates of the interface for each ply and $\overline{\underline{\hat{\boldsymbol{C}}}}_k$ denotes the *rotated* in-plane stiffness matrix for ply k. The local stiffness matrices are rotated using transformation matrices $\underline{\boldsymbol{T}}_1$ and $\underline{\boldsymbol{T}}_2$ as

$$\overline{\underline{\hat{\boldsymbol{C}}}} = \underline{\boldsymbol{T}}_1^{-1}\, \underline{\hat{\boldsymbol{C}}}\, \underline{\boldsymbol{T}}_2 \tag{3.11}$$

with the transformation matrices defined as

$$\underline{\boldsymbol{T}}_1 = \begin{bmatrix} \cos^2\theta & \sin^2\theta & 2\sin\theta\cos\theta \\ \sin^2\theta & \cos^2\theta & -2\sin\theta\cos\theta \\ -\sin\theta\cos\theta & \sin\theta\cos\theta & \cos^2\theta - \sin^2\theta \end{bmatrix} \tag{3.12}$$

$$\underline{\boldsymbol{T}}_2 = \begin{bmatrix} \cos^2\theta & \sin^2\theta & \sin\theta\cos\theta \\ \sin^2\theta & \cos^2\theta & -\sin\theta\cos\theta \\ -2\sin\theta\cos\theta & 2\sin\theta\cos\theta & \cos^2\theta - \sin^2\theta \end{bmatrix} \tag{3.13}$$

where θ is the angle between the veneer fiber direction and the global x-axis of the entire laminate.

For out-of-plane shear the corresponding assembled stiffness is given by

$$\underline{\tilde{\boldsymbol{A}}} = \sum_{k=1}^{N} \overline{\underline{\tilde{\boldsymbol{C}}}}_k (h_k - h_{k-1}) \tag{3.14}$$

with rotated out-of-plane stiffness

$$\overline{\underline{\tilde{\boldsymbol{C}}}} = \underline{\tilde{\boldsymbol{T}}}_1^{-1}\, \underline{\tilde{\boldsymbol{C}}}\, \underline{\tilde{\boldsymbol{T}}}_1 \tag{3.15}$$

and the associated transformation matrix

$$\underline{\tilde{\boldsymbol{T}}}_1 = \begin{bmatrix} \cos\theta & -\sin\theta \\ \sin\theta & \cos\theta \end{bmatrix} \tag{3.16}$$

It is noted that for 0° plies the transformation matrices are equal to identity meaning that the global- (xy) and ply (LT) coordinate systems coincide, implying that the rotated and local stiffness matrices are equal

$$\overline{\underline{\hat{\boldsymbol{C}}}}(\theta = 0) = \underline{\hat{\boldsymbol{C}}}, \qquad \overline{\underline{\tilde{\boldsymbol{C}}}}(\theta = 0) = \underline{\tilde{\boldsymbol{C}}} \tag{3.17}$$

The $\underline{\boldsymbol{A}}$, $\underline{\boldsymbol{B}}$, $\underline{\boldsymbol{D}}$ and $\underline{\tilde{\boldsymbol{A}}}$ matrices are used to express the response in terms of forces and moments as

$$\begin{bmatrix} \underline{\boldsymbol{F}} \\ \underline{\boldsymbol{M}} \end{bmatrix} = \begin{bmatrix} \underline{\boldsymbol{A}} & \underline{\boldsymbol{B}} \\ \underline{\boldsymbol{B}} & \underline{\boldsymbol{D}} \end{bmatrix} \begin{bmatrix} \underline{\boldsymbol{\varepsilon}}^0 \\ \underline{\boldsymbol{\kappa}} \end{bmatrix}, \qquad \underline{\boldsymbol{R}} = \underline{\tilde{\boldsymbol{A}}}\, \underline{\boldsymbol{\gamma}}_3 \tag{3.18}$$

where $\underline{\boldsymbol{F}}$, $\underline{\boldsymbol{M}}$ and $\underline{\boldsymbol{R}}$ are the loads (per unit length) representing in-plane extensional forces and moments and out-of-plane shear forces respectively. The in-plane deformations $\underline{\boldsymbol{\varepsilon}}^0$ and $\underline{\boldsymbol{\kappa}}$ represent mid-plane strains and curvatures and $\underline{\boldsymbol{\gamma}}_3$ denote the out-of-plane shear strains. The individual components are given as

$$\underline{\boldsymbol{F}} = \begin{bmatrix} F_1 \\ F_2 \\ F_{12} \end{bmatrix}, \qquad \underline{\boldsymbol{\varepsilon}}^0 = \begin{bmatrix} \varepsilon_1^0 \\ \varepsilon_2^0 \\ \gamma_{12}^0 \end{bmatrix} \tag{3.19}$$

$$\underline{\boldsymbol{M}} = \begin{bmatrix} M_1 \\ M_2 \\ M_{12} \end{bmatrix}, \qquad \underline{\boldsymbol{\kappa}} = \begin{bmatrix} \kappa_1 \\ \kappa_2 \\ \kappa_{12} \end{bmatrix} \tag{3.20}$$

$$\underline{\boldsymbol{R}} = \begin{bmatrix} R_{23} \\ R_{13} \end{bmatrix}, \qquad \underline{\boldsymbol{\gamma}}_3 = \begin{bmatrix} \gamma_{23} \\ \gamma_{13} \end{bmatrix} \tag{3.21}$$

Note that the presented laminate theory is based on the assumptions in Kirchhoff-Love plate theory, which is applicable for thinner plates. Therefore the theory become a less accurate approximation for thicker members (the σ_3 component of the stress is no longer negligible). Only thinner laminates are studied using laminate theory in this work. For the full scale structure of the wind turbine tower one must make sure that the plate assumptions are applicable.

3.3 Kerto-Q analysis

Since the stiffness parameters are known only for standardized LVL-sheets and not the particular layup used by Modvion, it is desired to predict the properties of an individual veneer. The aim is to assess any layup from the veneer properties using laminate theory. Since Kerto-Q and Modvion's sheets share several properties (Section 2.2), the approach to describe the material behaviour of the LVL modules is to evaluate the laminate stiffness parameters of a Kerto-Q sheet. The data for the evaluated Kerto-Q product is presented in Table 3.1, where N_0 and N_{90} are the number of 0° and 90° veneers and t is the total thickness of the laminate.

Table 3.1: Geometrical data for Kerto-Q.

t [mm]	Layup	N	N_0	N_{90}
27	$[0/90/0_2/\bar{0}]_s$	9	7	2

3.3.1 Laminate averaging

When designing LVL structures according to Eurocode 5 the variability of stiffness within the material through the thickness is considered using a mean stiffness for the whole laminate [13]. The mean laminate properties are determined from ideal tension, compression, bending and shear tests on an assembled laminate in accordance with Eurocode 5. The tests only consider strain in the direction of the load, as a consequence the stiffness parameters are simplified such that the coupling between strains are neglected, resulting in an uncoupled stress-strain relation. With these simplifications the constitutive relation can be written as

$$\begin{bmatrix} \sigma_1 \\ \sigma_2 \\ \sigma_{23} \\ \sigma_{13} \\ \sigma_{12} \end{bmatrix} = \begin{bmatrix} E_1 & 0 & 0 & 0 & 0 \\ 0 & E_2 & 0 & 0 & 0 \\ 0 & 0 & G_{23} & 0 & 0 \\ 0 & 0 & 0 & G_{13} & 0 \\ 0 & 0 & 0 & 0 & G_{12} \end{bmatrix} \begin{bmatrix} \varepsilon_1 \\ \varepsilon_2 \\ \gamma_{23} \\ \gamma_{13} \\ \gamma_{12} \end{bmatrix} \tag{3.22}$$

where the non-zero components in the constitutive matrix are mean values and the neglected coupling terms are zero.

A symmetric layup, equally thick veneers and the 0°/90° veneer directions of the standardized layups enable simplifications to the expressions given in Section 3.2. Symmetry of the laminate entails that all components of the coupling matrix $\underline{\boldsymbol{B}}$ are equal to zero (Eqs. (3.10) and (3.18)). This means there is no relation between in-plane extensional deformations and bending. Furthermore all standardized LVL products as well as the sheets used by Modvion consist of veneers of equal thickness. Equally thick veneers combined with fiber directions of only 0° and 90° entails that the individual stiffness components of the assembled laminate can be expressed as

$$C_{11}^* = \frac{N_0\, C_{11} + N_{90}\, C_{22}}{N}, \qquad C_{12}^* = C_{12}, \qquad C_{22}^* = \frac{N_{90}\, C_{11} + N_0\, C_{22}}{N} \tag{3.23}$$

$$C_{44}^* = \frac{N_0\, C_{44} + N_{90}\, C_{55}}{N}, \qquad C_{55}^* = \frac{N_{90}\, C_{44} + N_0\, C_{55}}{N}, \qquad C_{66}^* = C_{66} \tag{3.24}$$

where stiffness components denoted with * represent the weighted stiffnesses of the entire laminate, based on the relation between the number of 0° veneers and the number of 90° veneers. The average laminate stress can therefore be expressed in terms of a weighted laminate stiffness matrix and the average laminate strain

$$\begin{bmatrix} \sigma_1 \\ \sigma_2 \\ \sigma_{23} \\ \sigma_{13} \\ \sigma_{12} \end{bmatrix} = \begin{bmatrix} C_{11}^* & C_{12}^* & 0 & 0 & 0 \\ C_{12}^* & C_{22}^* & 0 & 0 & 0 \\ 0 & 0 & C_{44}^* & 0 & 0 \\ 0 & 0 & 0 & C_{55}^* & 0 \\ 0 & 0 & 0 & 0 & C_{66}^* \end{bmatrix} \begin{bmatrix} \varepsilon_1 \\ \varepsilon_2 \\ \gamma_{23} \\ \gamma_{13} \\ \gamma_{12} \end{bmatrix} \tag{3.25}$$

Using the relation in Eq. (3.7) it is possible to establish an additional equality between the longitudinal and transversal weighted stiffnesses C_{11}^* and C_{22}^* and the coupling term C_{12}^* as

$$C_{12}^* = \nu_{12}\, C_{22}^* = \nu_{21}\, C_{11}^* \tag{3.26}$$

3.3.2 Back calculation

The stiffness of individual veneers can be calculated from properties of an assembled laminate. This calculation procedure is referred to as *back calculation* of the veneer stiffness properties, since equations are commonly used to determine laminate properties from veneers rather than veneer properties from a laminate. When evaluating the stiffness for individual veneers from an assembled laminate, the effect of adhesion between veneers is included. Consequently the back calculated stiffnesses are regarded as *equivalent* properties of the particular veneer and adhesive used in the studied layup. This is considered a benefit since the effect of lamination is difficult to model and incorporate on values for the raw material. The back calculation is performed on laminates from two different data sources and are presented in Table 3.2.

Table 3.2: Tested stiffness parameters for Kerto-Q.

Data source	E_1 [MPa]	E_2 [MPa]	G_{12} [MPa]	G_{13} [MPa]	G_{23} [MPa]	ν_{21} [-]
Metsä Wood [18]	10500	2400	600	120	22	-
Tlustochowicz [19]	10590	2967	500	147.5	48.9	0.02

The tabulated stiffnesses are mean values taken from the LVL producer Metsä Wood and the PhD thesis of Tlustochowicz. Note that Poisson's ratio is not available from the Metsä Wood data source and that the stiffnesses are the averaged values for the entire laminate for both sources.

The back calculating of veneer properties is based on the assumption that the mean stress for the uncoupled relation and the average laminate stress are equal. Using this assumption it is possible to directly solve for the individual shear stiffnesses C_{44}, C_{55} and C_{66}. Since the in-plane shear is uncoupled from the other stresses and strains, it is noted that the method will result in equal values for the local stiffness C_{66} and the tested mean value G_{12}. The analytical relation used to solve for C_{44} and C_{55} is defined as

$$\begin{cases} C_{44} = \dfrac{N G_{23} - N_{90}\, C_{55}}{N_0} \\ C_{55} = \dfrac{N(N_0\, G_{13} - N_{90}\, G_{23})}{N_0^2 - N_{90}^2} \end{cases} \tag{3.27}$$

The resulting shear stiffnesses from the back calculation are presented in Table 3.3.

Table 3.3: Resulting shear stiffnesses from the back calculation.

Data source	C_{44} [MPa]	C_{55} [MPa]	C_{66} [MPa]
Metsä Wood	-17	159	600
Tlustochowicz	9	187	500

To solve for the in-plane stiffnesses C_{11}, C_{12} and C_{22}, a numerical solver is used due to the complexity of the equations. For the data from Tlustochowicz, Eq. (3.26) was utilized to establish a uniquely determined set of equations, where the resulting minimization routine is given as

$$\begin{aligned} \min_{C_{11}, C_{22}} \quad & \left(\frac{N_0\, C_{11} + N_{90}\, C_{22}}{N} - \frac{N \nu_{21}^2 \left(\dfrac{N_0\, C_{11} + N_{90}\, C_{22}}{N} \right)^2}{N_{90}\, C_{11} + N_0\, C_{22}} - E_1 \right)^2 + \\ & \left(- \frac{N \nu_{21}^2 \left(\dfrac{N_0\, C_{11} + N_{90}\, C_{22}}{N} \right)^2}{N_0\, C_{11} + N_{90}\, C_{22}} + \frac{N_{90}\, C_{11} + N_0\, C_{22}}{N} - E_2 \right)^2 \end{aligned} \tag{3.28}$$

For the data from Metsä Wood the absence of major Poisson's ratio entail an undetermined system of equations. The following routine was used to solve the modified minimization

$$\begin{aligned} \min_{C_{11}, C_{12}, C_{22}} \quad & \left(\frac{N_0\, C_{11} + N_{90}\, C_{22}}{N} - \frac{N C_{12}^2}{N_{90}\, C_{11} + N_0\, C_{22}} - E_1 \right)^2 + \\ & \left(- \frac{N C_{12}^2}{N_0\, C_{11} + N_{90}\, C_{22}} + \frac{N_{90}\, C_{11} + N_0\, C_{22}}{N} - E_2 \right)^2 \end{aligned} \tag{3.29}$$

Two sets of optimization routines are performed to approximately solve for the in-plane stiffnesses. The first case allows any value for the optimized variables and the second include the constraint that all variables should be greater than or equal to zero. Table 3.4 and 3.5 show the resulting axial stiffnesses C_{11} and C_{22} for the constrained and unconstrained optimization.

Table 3.4: Resulting optimized values for C_{11} [MPa].

Minimization condition	constrained	unconstrained
Metsä Wood	15349	17562
Tlustochowicz	13615	13695

Table 3.5: Resulting optimized values for C_{22} [MPa].

Minimization condition	constrained	unconstrained
Metsä Wood	0	-1074
Tlustochowicz	0	-82

The residual of the optimization is used to quantify the condition of the minimized values. It is calculated as the value of the expressions in Eqs. (3.28) and (3.29) for the minimized parameters. The resulting residuals are presented in Table 3.6.

Table 3.6: Residual from optimization [MPa^2].

Minimization condition	constrained	unconstrained
Metsä Wood	$3.3 \cdot 10^5$	$1.7 \cdot 10^{-11}$
Tlustochowicz	$3.2 \cdot 10^3$	$9.5 \cdot 10^{-10}$

From the resulting stiffness parameters it is apparent that using the approach of back calculating the equivalent veneer properties is not an appropriate method, for the studied data sets. Both the analytically solved shear stiffnesses and the optimized in-plane stiffnesses result in non-physical, negative values. The constrained optimization result in stiffnesses equaling zero as well as a significantly larger residual than for the unconstrained solution, indicating the minimum property of the unconstrained solution. It can thus be assumed that the method of back calculating the equivalent veneer properties is an unfit approach with the set of equations and material parameters used.

3.4 Assembling from raw material

Instead of determining the veneer properties from back calculating a standardized product, data for the raw material can be used to describe the veneers. The drawback of this method is the loss of the effect from lamination, included in the equivalent values achieved from the back calculation. Raw material properties from ultrasonic testing of three specimens of European softwood spruce [20] is presented in Table 3.7. Both data for the sub-scale parameters as well as the associated components of the Hooke tensor is included. The data was evaluated for cubical test specimens with an edge length of 20 mm, cut from the tree such that the influence of the growth rings curvature is negligible. Therefore it is assumed to represent clearwood or material completely free of defects.

Table 3.7: Data from ultrasonic testing of softwood spruce [20].

Components in Hooke tensor [MPa]								
C_{11}	C_{12}	C_{13}	C_{22}	C_{23}	C_{33}	C_{44}	C_{55}	C_{66}
17420	1720	1555	2390	1180	1940	74	910	940

Sub-scale parameters [MPa]			
E_L	E_T	ν_{LT}	ν_{TL}
15810	1640	0.466	0.048

To be able to compare with the back calculated values, the same layup (presented in Table 3.1) was used for the assembly. The analysis is performed with and without the assumption that σ_3 equals zero, i.e. with the full 6×6 $\underline{\boldsymbol{C}}$-matrix and with C_{13}, C_{23} and C_{33} components being neglected. In the constitutive relation (Eq. (3.4)) the values for the shear components C_{44}, C_{55} and C_{66} are uncoupled, meaning they are independent of the σ_3 assumption. As mentioned in Section 3.3.2 the in-plane shear stiffness is equal on the veneer and laminate scale, since the laminate consist of only 0° and 90° veneers. The result from the assembly using the raw material data is presented in Table 3.8.

Table 3.8: Assembled stiffnesses from ultrasonic data.

Uniaxial components [MPa]		
Size of $\underline{\boldsymbol{C}}$	E_1	E_2
5×5	12827	4852
6×6	13562	5518
Shear components [MPa]		
G_{12}	G_{13}	G_{23}
940	724	260

Due to the exclusion of the out-of-plane stiffness contribution, the assembled values for E_1 and E_2 are slightly lower with the σ_3 assumption. Note that the results give a higher prediction of the stiffness than the tested values from Table 3.2.

4 Finite element analysis

The strategy to capture the veneer effect and homogenization described in Sections 2.3 and 2.5 is to create an FE-model. A 3D, linear elastic model is created to be able to analyse the load distribution in- and out-of-plane around knots, which a 2D model would not be able to. To compare different sizes of laminates the FE-model uses 0° and 90° veneers, alternated throughout the laminate, corresponding to the same layup pattern with increasing number of veneers for all studied layups.

For evaluation of the results the maximum relative stress in the x-direction is used, which is defined as the maximum longitudinal stress, $\sigma_{1,\max}$, divided by the corresponding stress for the ideal case, $\sigma_{1,\max,\text{ideal}}$, without defects or variation in veneer stiffness. The evaluated stress is always calculated as the mean over all Gauss points for each element. This quantity is chosen since it is comparable between the different layup sizes and independent of the magnitude of the applied load. It is noted that the stress for the ideal case is not equal for all models, since the number 0° veneers relative to the number of 90° veneers varies for the different layup sizes depending on the total number of veneers.

Geometrical properties for the studied layup sizes are presented in Table 4.1.

Table 4.1: Layup properties.

Size (i)	Layup	$t^{(i)}$ [m]	$N^{(i)}$
1	$[0/\bar{90}]_\text{s}$	$9 \cdot 10^{-3}$	3
2	$[(0/90)_2/\bar{0}]_\text{s}$	$27 \cdot 10^{-3}$	9
3	$[(0/90)_6/0/\bar{90}]_\text{s}$	$81 \cdot 10^{-3}$	27
4	$[(0/90)_{20}/\bar{0}]_\text{s}$	$243 \cdot 10^{-3}$	81

Layup 1 represent the thickness of the sheets used in the prototype tower, seen in Figure 1.2. Layup 2 represent the thickness of a sheet and Layup 4 the thickness of a module in the 150 m tower. Layup 3 is an intermediate step between the second and fourth.

Two different constitutive matrices, one for the 0° and one for the 90° veneers are used to describe the 3D solid. They are both the same material but their properties are different relative to the longitudinal axis of the laminate. The two versions of the constitutive element matrices $\underline{\boldsymbol{C}}_\text{E}$ are given as

$$\underline{\boldsymbol{C}}_{\text{E},0} = \begin{bmatrix} C_{11} & C_{12} & C_{13} & 0 & 0 & 0 \\ C_{12} & C_{22} & C_{23} & 0 & 0 & 0 \\ C_{13} & C_{23} & C_{33} & 0 & 0 & 0 \\ 0 & 0 & 0 & C_{44} & 0 & 0 \\ 0 & 0 & 0 & 0 & C_{55} & 0 \\ 0 & 0 & 0 & 0 & 0 & C_{66} \end{bmatrix}, \qquad \underline{\boldsymbol{C}}_{\text{E},90} = \begin{bmatrix} C_{22} & C_{12} & C_{23} & 0 & 0 & 0 \\ C_{12} & C_{11} & C_{13} & 0 & 0 & 0 \\ C_{23} & C_{13} & C_{33} & 0 & 0 & 0 \\ 0 & 0 & 0 & C_{55} & 0 & 0 \\ 0 & 0 & 0 & 0 & C_{44} & 0 \\ 0 & 0 & 0 & 0 & 0 & C_{66} \end{bmatrix} \tag{4.1}$$

It is noted that the assumption used in laminate theory, reducing the $\underline{\boldsymbol{C}}$ matrix from a 6×6 to a 5×5 matrix is omitted in the 3D model. The stiffness values used correspond to the Hooke tensor components from the ultrasonic testing, presented in Table 3.7. The ideal model without knot or veneer distribution is therefore also assumed to represent a clearwood specimen consisting of defect free raw material. Modeling of the cohesive zone in the interface between laminates is not performed since it is not in the scope of this work.

Homogenization and veneer effect are modeled separately, both for four cases of different thickness with the same uniformly distributed tensile load. For all cases a Monte Carlo simulation of ten thousand runs is performed.

4.1 3D model

The FE-analysis is based on a cuboid laminate subjected to tension in the longitudinal direction, simulating a uniaxial tension test. This model is chosen since the size effect is a phenomena for materials loaded in tension, as mentioned in Section 2.4. The modelling is performed in MATLAB[2] using the FE-toolbox CALFEM. Eight-node, cuboid, iso-parametric elements of equal size, with eight Gauss integration points each are used. Homogenization and veneer effect are included by modifying the element stiffness matrices, $\underline{\boldsymbol{K}}_{\mathrm{E}}$, equivalent of scaling the corresponding element constitutive matrix $\underline{\boldsymbol{C}}_{\mathrm{E}}$ (due to linear elasticity).

Veneers are modeled using a single element in the z-direction. The number of elements (NEL) in the x-direction, $N_{\mathrm{E},x}$, and y-direction, $N_{\mathrm{E},y}$, are kept constant, thus the total number of elements, N_{E}, is proportional to the number of veneers. A sketch of the model with load case and boundary conditions for the same example layup seen in Figure 3.1 is illustrated in Figure 4.1.

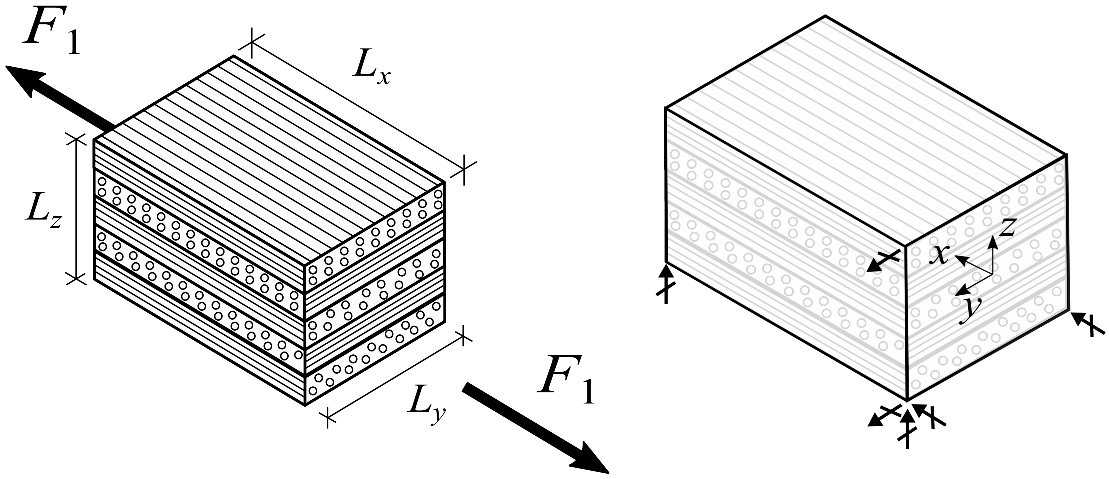

Figure 4.1: 3D model with boundary conditions for the example layup.

The load, F_1, is distributed evenly on the surfaces in the yz-plane and the boundary conditions are set according to the figure, preventing rigid body motion (RBM). Both the homogenization and veneer effect are modeled using a load case with a constant applied force, corresponding to a force controlled FE-problem. As a consequence the stresses at the boundaries where the force is applied are uniform, which is not a physical behavior in a cross section of varying stiffness. In an event that there is a knot at the boundary the variation will increase and this effect will be amplified even further. However, at a distance from the boundary the loads will have redistributed such that a more realistic stress distribution is reached in the cross section.

The assigned properties for the FE-model are presented in Table 4.2.

Table 4.2: Input for FE-model.

F_1 [Pa]	L_x [m]	L_y [m]	L_z [m]	$N_{\mathrm{E},x}$	$N_{\mathrm{E},y}$	$N_{\mathrm{E},z}$
$100 \cdot 10^6$	1	0.5	$t^{(i)}$	20	10	$N^{(i)}$

Where L_x, L_y and L_z are the cuboid dimensions according to Figure 4.1 and $N_{\mathrm{E},z}$ is the NEL in the z-direction, i.e. the number of veneers. The load F_1 is scaled using the constant depth L_y and the height L_z, depending on the size of the layup, resulting in the the same force relative to the cross section area for each layup. In the z-direction the NEL is always set as the number of veneers and the NEL in x- and y-direction were chosen corresponding to the model dimensions as

$$N_{\mathrm{E},x} = 2 \cdot N_{\mathrm{E},y} \tag{4.2}$$

[2]Matlab, version R2019b, Numerical computing environment

4.2 Convergence study

To verify that the mesh resolution is sufficiently refined and provides a converged solution, a convergence study is performed for the ideal case with no homogenization or veneer effect for each separate layup. The convergence was only evaluated for varying NEL in the xy-plane, consequently the influence of $N_{\mathrm{E},z}$ is not studied. Convergence is evaluated through the energy norm, $||\bullet||$, for the solution on different meshes and compare the result in terms of the relative error (RE), φ

$$\varphi = \frac{||\boldsymbol{e}||}{||\boldsymbol{u}||} \tag{4.3}$$

where the exact solution, $\boldsymbol{u}$, is approximated as the solution for an assumed overkill mesh of $968 \times N_{\mathrm{E},z}$ elements. The energy norm of the error, $\boldsymbol{e}$, is evaluated from the exact and FE-solution as

$$||\boldsymbol{e}|| = \sqrt{||\boldsymbol{u}||^2 - ||\boldsymbol{u}_h||^2} \tag{4.4}$$

with the energy norm expressed in terms of the FE-solution or displacement vector, $\underline{\boldsymbol{a}}$, and global stiffness matrix, $\underline{\underline{\boldsymbol{K}}}$, as

$$||\boldsymbol{u}_h|| = \sqrt{\underline{\boldsymbol{a}}^{\mathrm{T}}\underline{\underline{\boldsymbol{K}}}\,\underline{\boldsymbol{a}}} \tag{4.5}$$

Figure 4.2 presents the result from the convergence study.

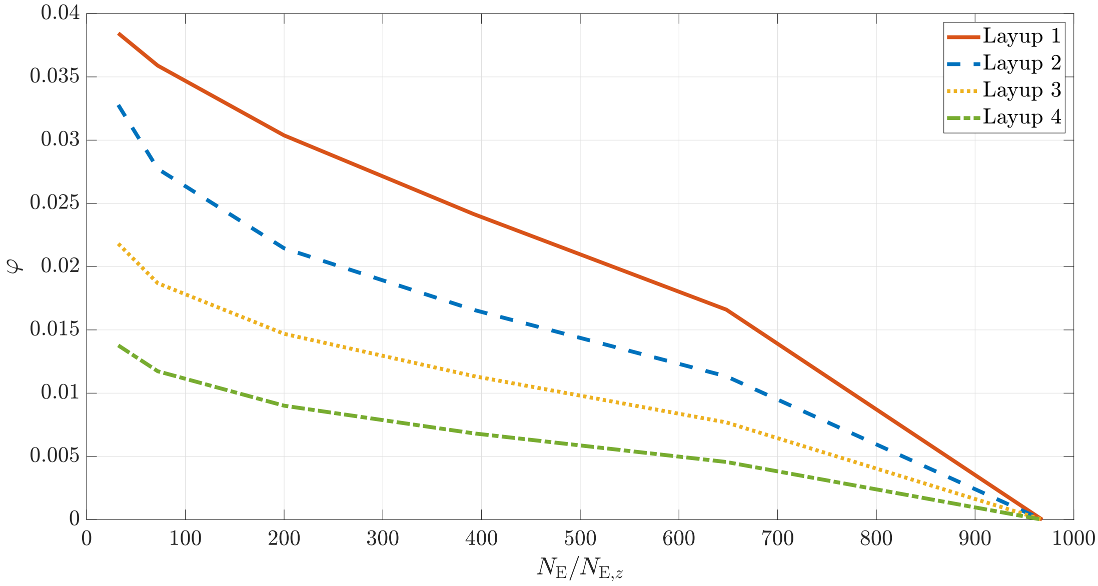

Figure 4.2: Convergence of the relative error versus number of elements for each layup size.

It is observed that the chosen mesh corresponding to the values for $N_{\mathrm{E}}/N_{\mathrm{E},z} = 200$ results in a maximum relative error of approximately 3%.

4.3 Modeling veneer effect

The laminate consists of veneers, each having a stiffness $\underline{\boldsymbol{C}}_{\mathrm{E},0}$ or $\underline{\boldsymbol{C}}_{\mathrm{E},90}$ (Eq. (4.1)), which in reality will have a variation from production as mentioned in Section 4.3. To model this variation a modified constitutive element matrix $\underline{\boldsymbol{C}}_{\mathrm{E},\alpha}$ where, α, is a factor modifying $\underline{\boldsymbol{C}}_{\mathrm{E}}$ to be stiffer or less stiff

$$\underline{\boldsymbol{C}}_{\mathrm{E},\alpha} = \alpha\, \underline{\boldsymbol{C}}_{\mathrm{E}} \tag{4.6}$$

It is thus assumed that all stiffness parameters in the constitutive matrix of the veneers varies linearly by the same factor α. For each veneer, α is based on the coefficient of variation, c_{v}, corresponding to a Lognormal probabilistic model of the bending modulus for structural timber [7].

The expression for a Lognormal distribution is given in terms of the logarithmic parameters for the standard deviation, δ, and the mean, μ, as

$$p(\alpha) = \frac{1}{\alpha}\frac{1}{\delta\sqrt{2\pi}} \exp\left(-\frac{(\ln\alpha - \mu)^2}{2\delta^2}\right) \tag{4.7}$$

The distribution is created using the following expressions for δ, μ and the variance, v

$$\delta = \sqrt{\ln\left(\frac{v}{1+m^2}\right)}, \qquad \mu = \ln\left(\frac{m^2}{\sqrt{m^2+v}}\right), \qquad v = (c_{\mathrm{v}}\, m)^2 \tag{4.8}$$

with the values for the coefficient of variation and the mean

$$c_{\mathrm{v}} = 0.13, \qquad m = 1 \tag{4.9}$$

The probability density function (PDF) and the cumulative distribution function (CDF) of α is presented in Figure 4.3.

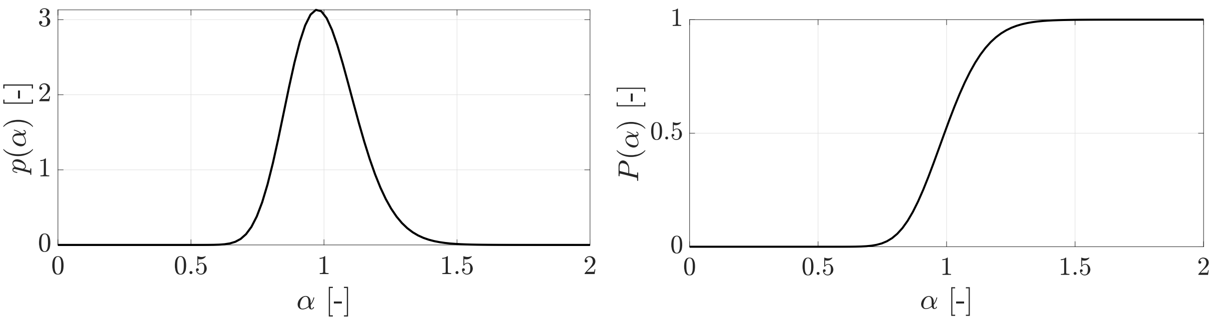

a Probability density function.

b Cumulative distribution function.

Figure 4.3: Lognormal distribution of veneer variability factor α.

The Lognormal distribution of α is used to modify the stiffness matrix for each veneer in all four studied layups.

4.4 Veneer effect simulation results

In order to avoid the non-physical material behaviour at the boundaries (Section 4.1), the results from the veneer effect model is evaluated in the middle cross section of the laminate. The resulting distributions for the veneer effect simulation can be seen in Figure 4.4, using a constant width of the data bins, λ.

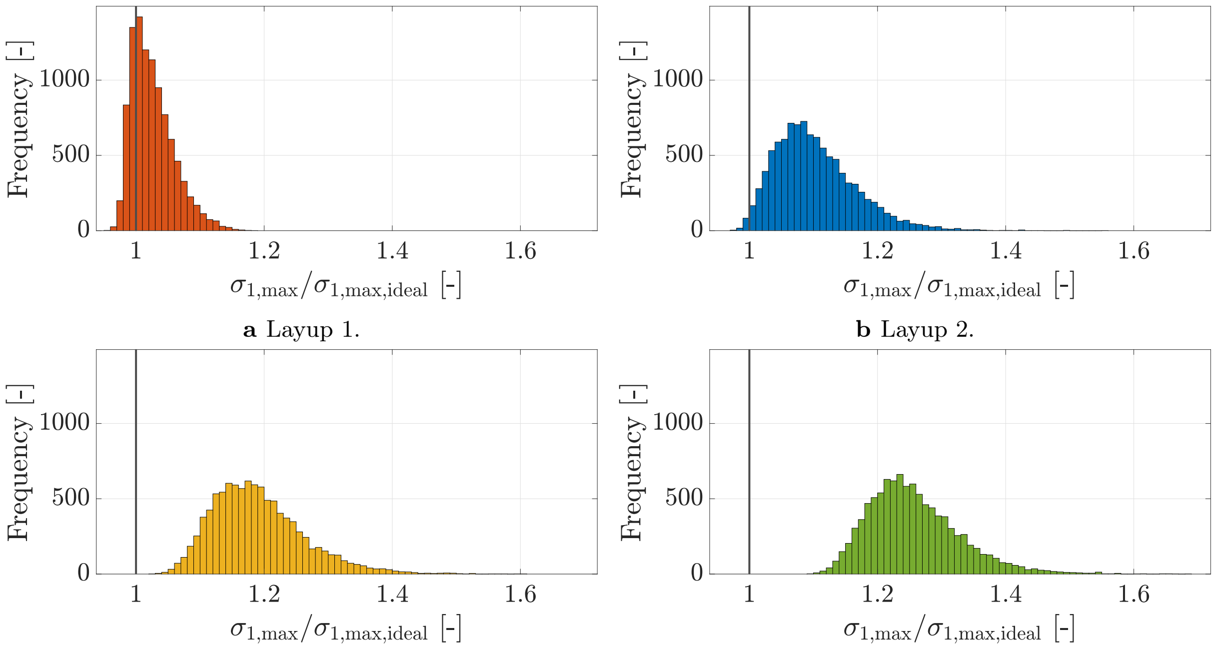

a Layup 1. **b** Layup 2. **c** Layup 3. **d** Layup 4.

Figure 4.4: Maximum relative stress for the veneer effect simulation, $\lambda = 0.01$.

An empirical PDF for each of the four distributions above is presented in Figure 4.5.

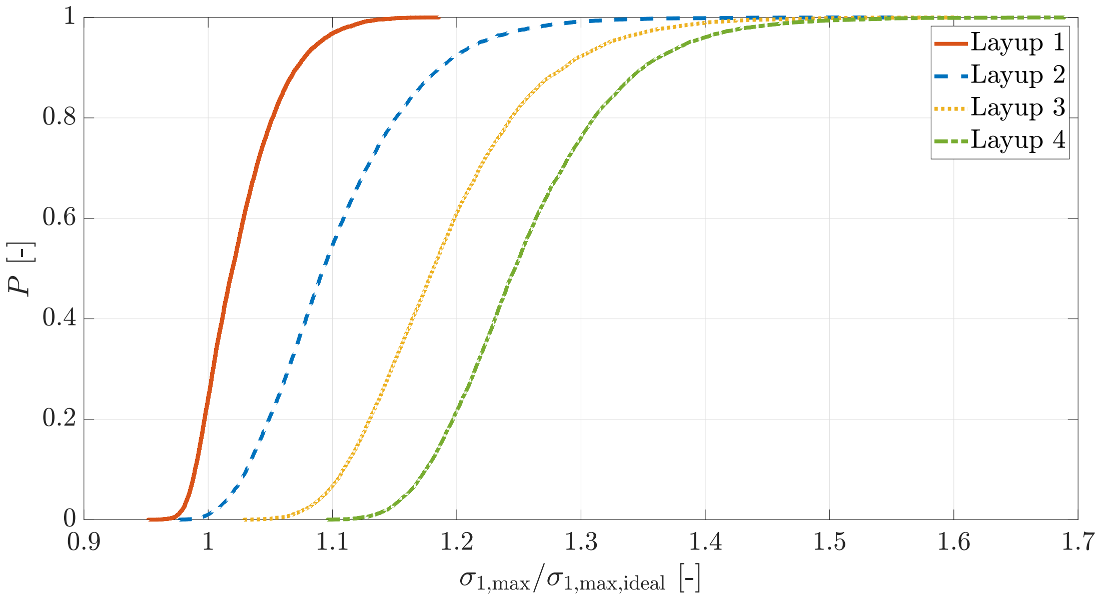

Figure 4.5: Empirical probability density functions for the veneer effect simulations.

From Figures 4.4 and 4.5 it is observed that the maximum relative stress from each Monte Carlo simulation increases with the layup thickness. In addition the variability of the distribution increase with the thickness of the layups.

4.5 Modeling homogenization

Wood is strongest in the direction of the fibers and if there is a knot in the material, the fibers deviate from its main direction and thus the strength and stiffness in the main fiber direction is lowered [3]. Therefore the influence of knots is important when modeling structural timber and EWP. Previous research have modeled defects by changing the fiber direction around knots [15, 21], where [15] also considers the knot itself to be a hole. An alternative approach models knots in Glulam beams by reducing the stiffness of the elements where knots are present [22].

The model created to study the homogenization uses the same mesh as for the veneer effect. Monte Carlo simulations are performed where a randomised knot distribution is determined for each run. The knots are of equal size and are modeled as voids in the material similar to [15]. In addition the knots are implemented in the model by reducing the stiffness of the elements containing knots as in [22].

Strips in the y-direction of each veneer, containing a statistically determined number of knots is used to decide the location of defects. The knot distribution intends to resemble the patterns created from production mentioned in Section 2.1. Outside the strips the material is considered knot free and the distance between strips is determined using a distance, d. The strips are assigned by considering the length of an element in the x-direction, meaning that the randomised strip location is related to the FE mesh-discretization. A principal sketch of how knots are included in the model for a three veneer laminate is illustrated in Figure 4.6.

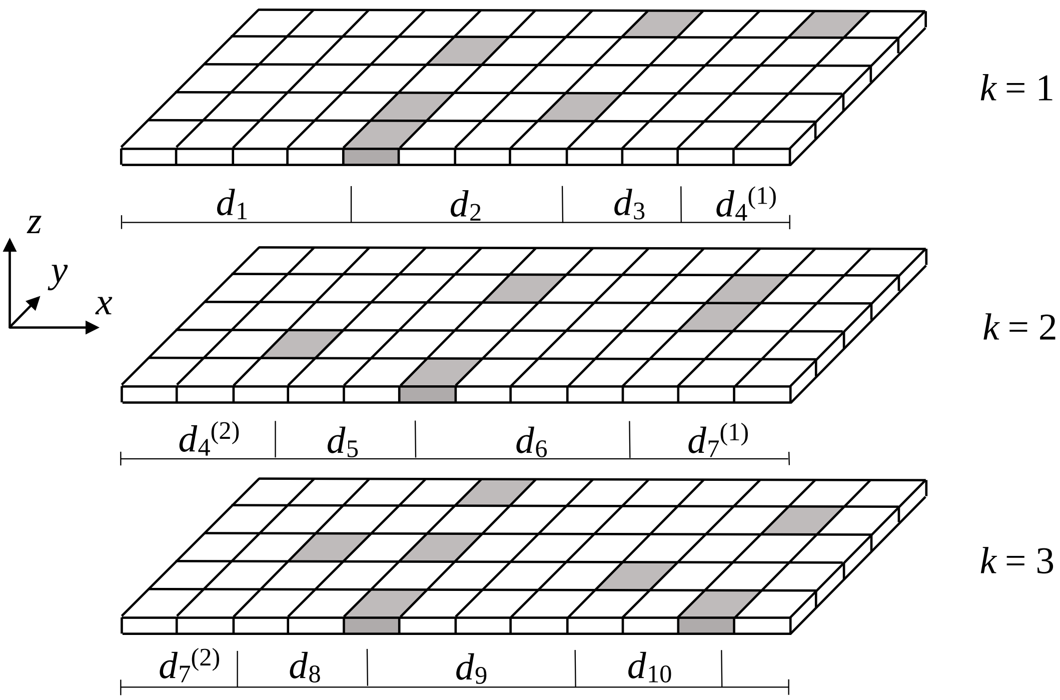

Figure 4.6: Principal sketch of a meshed, three veneer laminate. The gray elements are the location of each knot, which are considered stiffness free.

At the edges the distance d_4 and d_7 are split and continues in the next veneer ($k+1$), where $d_j = d_j^{(1)} + d_j^{(2)}$. In each strip a random number of knots; one, two or three is assigned. Each knot is considered stiffness free, modeled as an element that provides no stiffness in order to simulate a void. This also means that all knots will have the shape of one element, which is a cuboid with volume $50\,\text{mm} \times 50\,\text{mm} \times 3\,\text{mm}$. As mentioned in Section 2.5 the actual presence of defects will be cut sections of knots distributed as strips.

The knot free distance d varies according to the Gamma distribution defined in [22] as

$$p(d) = \frac{\nu\Big(\nu\big(d - L_{\mathrm{E},x}\big)\Big)^{w-1}}{\Gamma\big(w\big)} \exp\Big(- \nu\big(d - L_{\mathrm{E},x}\big)\Big) + L_{\mathrm{E},x} \tag{4.10}$$

where w and ν are positive constants. $L_{\mathrm{E},x}$ is the element length with constant value of 50 mm, corresponding to the minimum value of d. The Gamma function is defined as

$$\Gamma(w) = \int_0^\infty t^{w-1} \exp(-t) dt \tag{4.11}$$

with the values for the Gamma parameters w and ν

$$w = 2.37, \qquad \nu = 0.0063 \tag{4.12}$$

The values are taken from [22] and are a mean for boards of two strength grades of structural timber, where w is a statistical parameter and ν is Poisson's ratio. The PDF and CDF of d is presented in Figure 4.7.

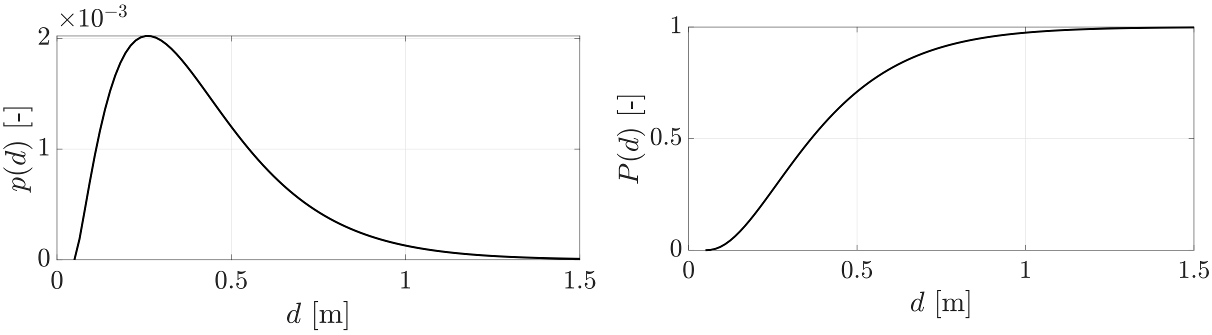

a Probability density function.

b Cumulative distribution function.

Figure 4.7: Gamma distribution of the knot free distance, d.

It is assumed that each knot is stiffness free, but in order to provide a stable FE-model, the element stiffness of knots is not set to zero. Instead the stiffness is reduced to such an extent that further reduction provides no significant change in the results. This is done by introducing a factor β, modifying all stiffness parameters in the constitutive element matrix, $\underline{\boldsymbol{C}}_{\mathrm{E}}$ according to

$$\underline{\boldsymbol{C}}_{\mathrm{E},\beta} = \beta\, \underline{\boldsymbol{C}}_{\mathrm{E}} \tag{4.13}$$

In order to find what factor β to be used such that the element stiffness does not further impact the results, a convergence study where β tends to zero is performed. The maximum relative stress introduced earlier is used as an indicator for when β does not further have to be reduced. Ten simulation runs of different knot distributions are performed for five different values of β. Table 4.3 show the values used for β and the convergence for all four layups is presented in Figure 4.8.

Table 4.3: Evaluated values of reduction factor β.

0.5	0.1	0.01	0.001	0.0001

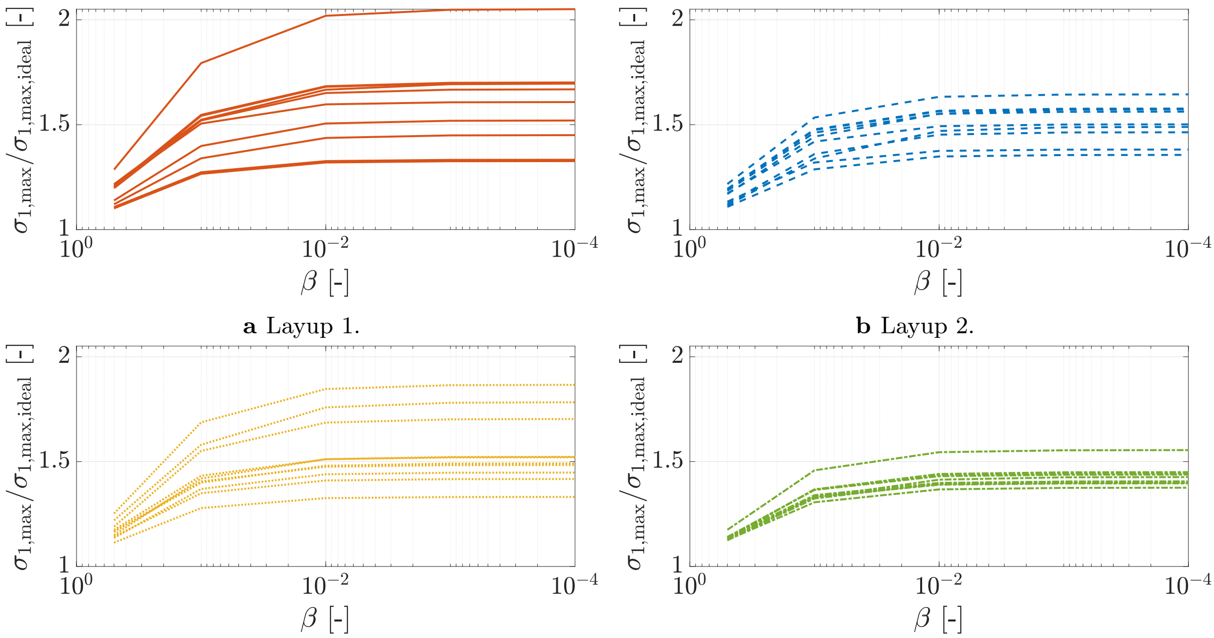

a Layup 1.

b Layup 2.

c Layup 3.

d Layup 4.

Figure 4.8: Lin-log plot of the maximum relative stress versus the reduction factor β for ten cases of knot distribution.

The results from the study of β show that the value 0.01 corresponds to a converged solution. A further decrease is considered negligible for all studied cases and consequently $\beta = 0.01$ is used in all further calculations.

4.6 Homogenization simulation results

In the homogenization simulation both the maximum and the 95% fractile of the relative stress is studied. In order to exclude results in the non-physical boundary where load is applied, the results from the homogenization simulation is evaluated for all elements at a minimum distance of 100 mm from the loaded boundaries. The simulation results for maximum relative stress in the homogenization model can be seen in Figure 4.9 and 4.10.

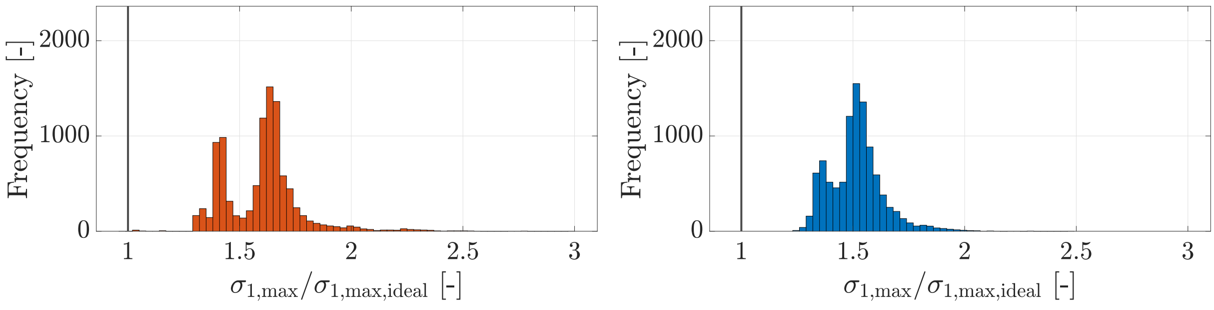

a Layup 1.

b Layup 2.

c Layup 3.

d Layup 4.

Figure 4.9: Maximum relative stress for the homogenization simulation, $\lambda = 0.03$.

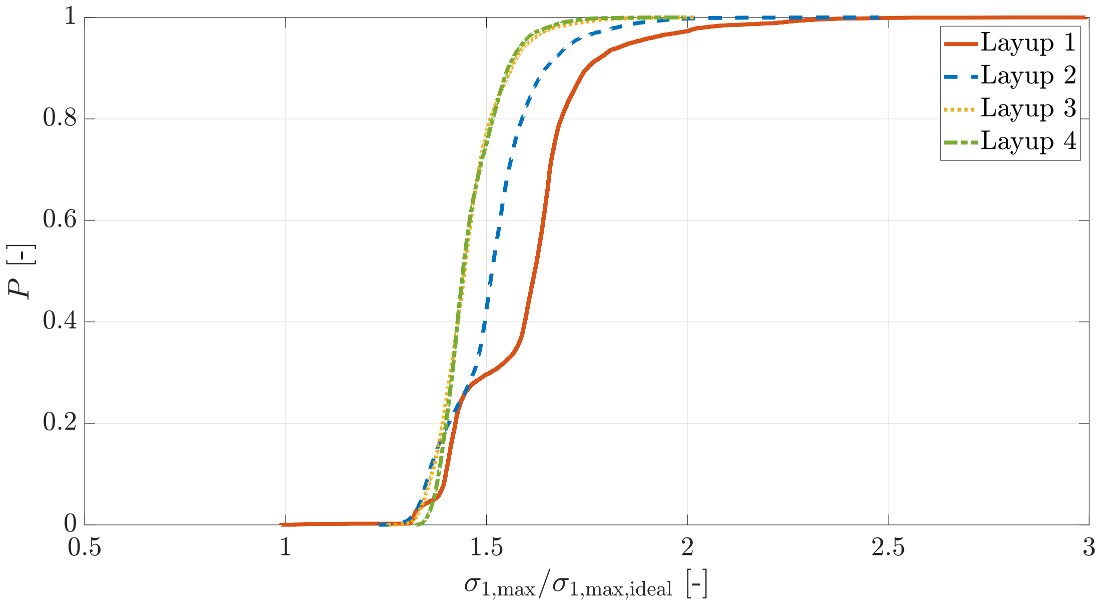

Figure 4.10: Empirical probability density functions of the maximum relative stress for the homogenization simulation.

Figure 4.9 show an instability in the maximum relative stress for Layup 1 and 2, where two separate peaks are observed in each distribution. This is not the case for the thicker layups having a more uniform distribution. Both the highest maximum relative stress and the mean are lower for the thicker layups. In this regard there is no significant difference between Layup 3 and 4. Note also that the lowest maximum relative stresses for all layups are more or less equal around a value of 1.3.

The results for the 95% fractile of the maximum relative stress is presented in 4.11 and 4.12.

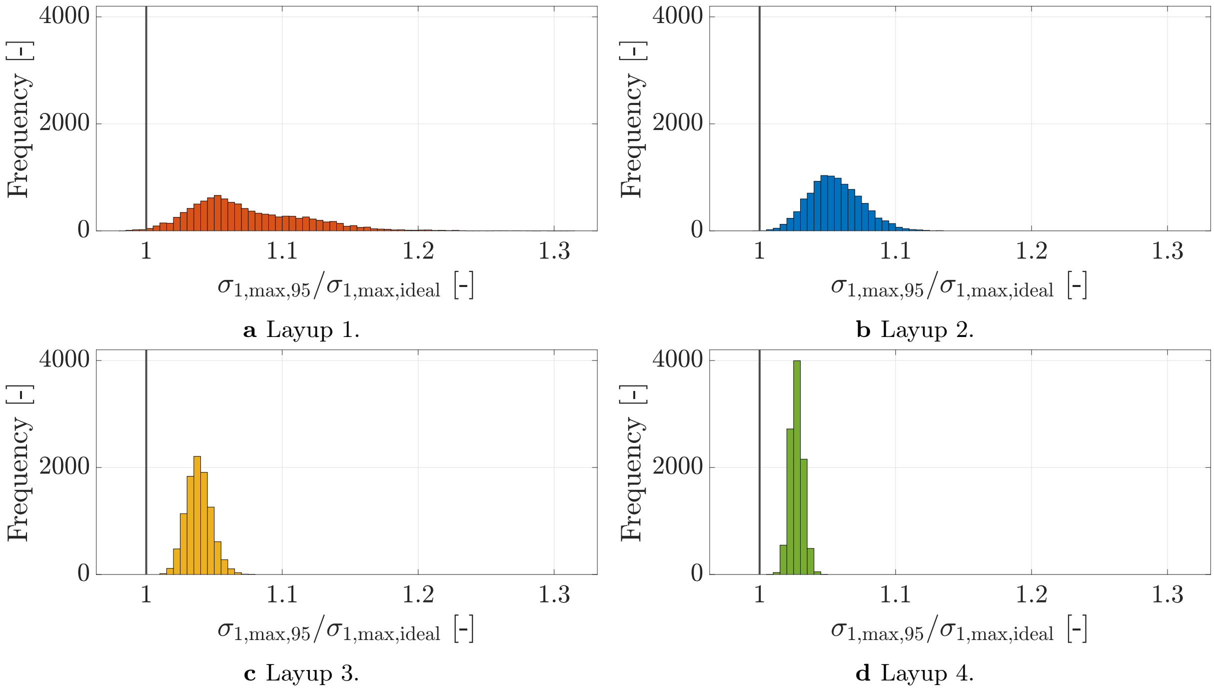

Figure 4.11: 95% fractile of the maximum relative stress for the homogenization simulation, $\lambda = 0.005$.

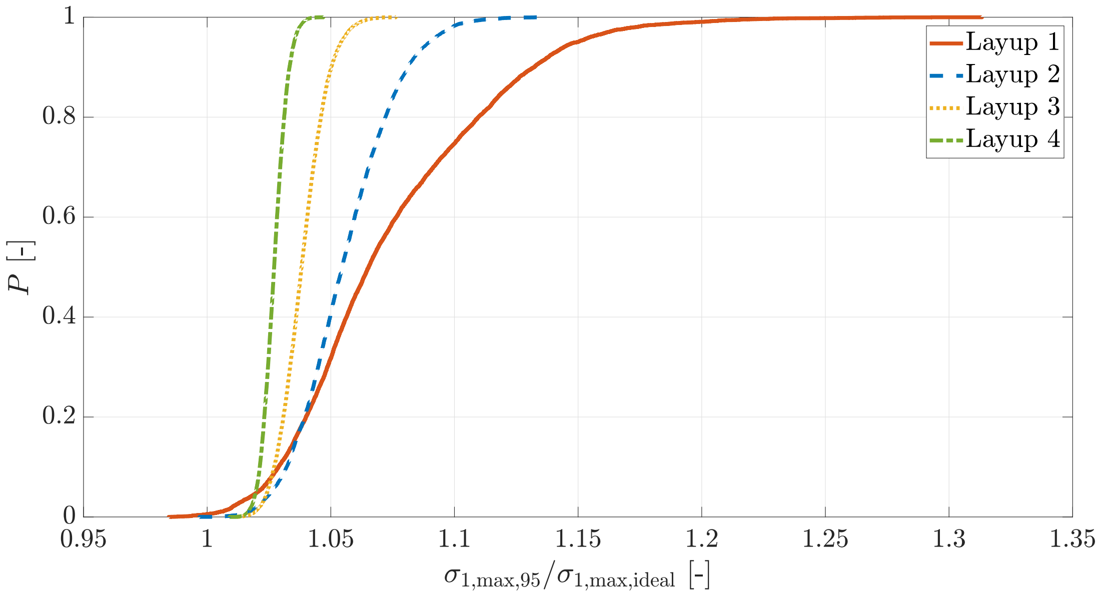

Figure 4.12: Empirical probability density functions for the 95% fractile of the maximum relative stress for the homogenization simulation.

For the 95% fractile Layup 1 show a high variability in results. As the thickness increases, the variability decreases. Comparing Layup 1 and 4, there is a significant difference in variability. In addition to a lower variability the thicker layups show lower relative stresses. Note that the lowest 95% fractile of the maximum relative stress does not have a minimum value of 1.3 as for the maximum relative stress. Here values are lower than one in some cases.

5 Discussion

The project have evaluated different properties of LVL in two major aspects; the possibility of using laminate theory to determine stiffness parameters and a 3D model investigating the elastic behaviour of thick LVL layups, containing defects and varying veneer stiffness. In this chapter the outcome of these studies are discussed.

5.1 Laminate modeling

The back calculation results in non-physical, negative values for some stiffness components, see Table 3.3 and 3.5. As mentioned in Section 3, the laminate theory used constitute simplifications such as; ideal bonding between veneers, perfectly aligned fibers and defect free material. In addition laminate theory neglects the σ_3-component and all coupling terms but C_{12}, relating the longitudinal to the transverse in-plane deformations. In the physical tests performed to determine the values in the uncoupled relation there is no quantification of the coupling between deformations. In reality each stress component has a dependence on strains in other directions. As a consequence the coupling terms in the constitutive matrix is neglected. Combining the different simplifications of laminate theory and the uncoupled relation can explain the non-physical results from the back calculation.

Furthermore, the data from Metsä Wood uses the same stiffness parameters for Kerto-Q products with thicknesses ranging from 27 mm to 75 mm, which indicates a rough estimation of the material parameters. This data is studied since it is what Modvion is using at the current time. Using alternative, more exact data may provide an improvement in the back calculation procedure.

The assembled values from the defect free raw material properties seen in Table 3.8 show higher stiffness values than both sources of the tested properties seen in Table 3.2. This is expected considering the effect of knots and lamination is not included.

5.2 3D modeling

In the FE-model one element per veneer is used in the z-direction and the mean stress of all Gauss points in each element is studied. This approach has the benefit of avoiding stress singularities in highly concentrated stress regions, compared to using a finer mesh discretization or evaluating stresses in individual Gauss points. In addition, a finer mesh discretization would increase the already long simulation time.

A force controlled FE-problem is chosen, which bring complications at the boundaries. An alternative to avoid this problem is to model a displacement controlled FE-problem, which would give realistic results in the entire domain, including the boundaries. The drawback of this method would be the loss of an identical reference load for any size of layup, instead the reference load would need to be approximated through iteration. Considering the additional effort of a displacement controlled model, a force controlled method with some restriction on where stresses are evaluated was chosen. In order to avoid non-physical results at the boundary, the stresses within a distance of 100 mm from the boundaries are not studied in the knot model. In the veneer model only the middle cross section is evaluated. The results from the veneer effect- and homogenization simulations are discussed in Section 5.2.1 and 5.2.2.

5.2.1 Veneer effect

Figure 4.4 show that the average magnitude of the maximum relative stress from each run of the Monte Carlo simulation is increased with the number of veneers. By studying the assigned values of α it is observed that the 0° veneers mainly governs the output, while the stiffness in the 90° veneers make small impact on the results. A 0° veneer with a high value of α in the vicinity of 0° veneers with a low α-value are the most critical, showing a high maximum relative stress, while more uniform distribution of α in the veneers gives lower maximum relative stresses. For Layup 4 the probability of a more critical stiffness distribution is higher, since the number of veneers, i.e. number of α-values is higher. This can explain the higher maximum relative stresses.

It is apparent that the variation in the maximum relative stress is lowest for Layup 1. Considering α for each veneer in the layup is randomized from the same distribution, the mean stiffness of all veneers in the Monte Carlo simulation will yield less variation for thicker laminates. From the simulation it is noted that this does not have a dominant effect on the stresses, indicating that the local stiffness variations in the laminate is governing for the maximum relative stress, i.e. a thicker laminate increases the probability of more critical local effects. Note that the results obtained for the veneer effect essentially would have been possible to obtain without the 3D model. Since each veneer is modified uniformly, a plate model can capture the same response for a given cross section.

5.2.2 Homogenization

Studying Figures 4.9 and 4.10 the lowest maximum relative stresses for all layups are more or less equal around a value of 1.3. This shows that any knot distribution will yield an increased maximum relative stress of about 30%, which is an indication that a knot free laminate will have a substantially lower highest stressed region, compared to a laminate containing knots. Note that the variation α is based on a probabilistic model of bending modulus of structural timber, which may differ from the stiffness variation of an LVL laminate.

Figure 4.10 and 4.12 show that the relative stresses in the thicker layups are lower compared to the thinner layups, with the exception being the very lowest maximum relative stresses around the 0.1 percentile region. For Layup 1 in Figure 4.11, the stress values occur in a wider range compared to the other layups.

Layup 1 and 2 in Figure 4.9 show an instability in the maximum relative stress distribution, where two distinct peaks can be observed. This is not the case for the thicker layups. By studying the knot distribution for a couple of samples, certain trends are observed. In general the highest relative stress increases with the total number of knots, in addition the knots in the 90° veneers show no particular trend. What happens in the 0° veneers seems to be governing for the highest stress and the highest stress always occurs in one of the 0° veneers, similar to the veneer effect. Note that only the loading case of pure tension is considered. For other load cases such as shear, the highest stress may occur in a 90° veneer.

The two different peaks for Layup 1 and 2 in Figure 4.9 can be explained through the knot distribution in the strips, where different trends are observed in both peaks. As mentioned in Section 4.1 a random number of knots (one, two or three) is included in each strip. Also the position of each knot within the strip is random and different knot patterns in the strip are more or less critical. For both peaks there are two to three knots in one of the two 0° veneers in proximity to the highest stress. What separates the right peak from the left is that the highest stressed elements are *jammed*, meaning two knots are located with a spacing of one element between them. Figure 5.1 show an example of the jammed case, which is the case for a majority of simulations in the peak on the right.

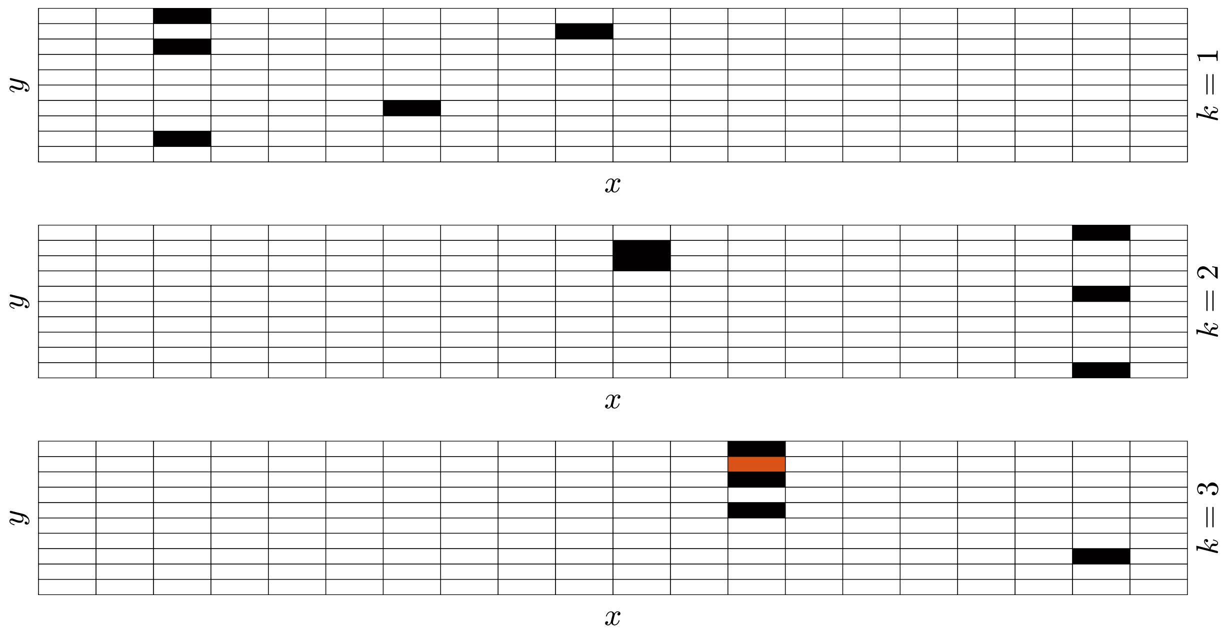

Figure 5.1: Example from the right peak of the distribution in Figure 4.9a.

Black elements are the locations of knots and the red element is the location of the highest stressed element. Figure 5.2 show the left peak, where there are no cases of jammed elements with maximum relative stress.

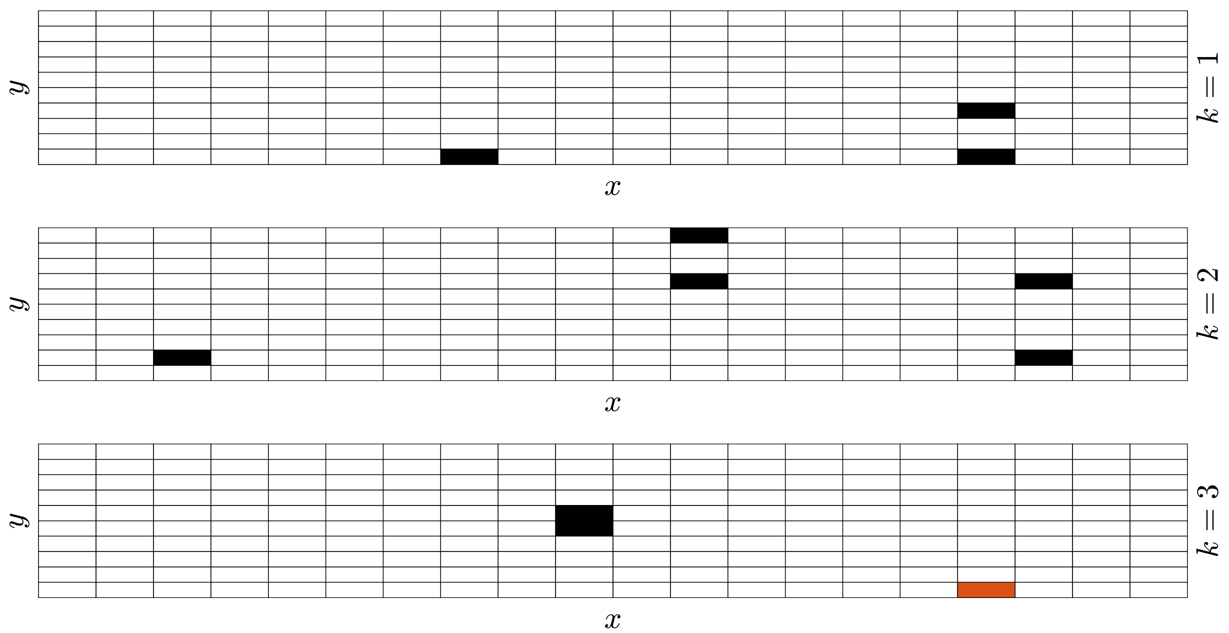

Figure 5.2: Example from the left peak of the distribution in Figure 4.9a.

For the thicker laminates in Layup 3 and 4, only one peak is present. Here the jammed elements occur consistently, explaining the more uniform curves.

The homogenization is modeled using strips of knots throughout the laminate according to Figure 4.6. All strips stretches in the same in-plane direction perpendicular to the direction of the applied load. This is a flaw in the model since in reality, as the transverse veneers are rotated the strips will rotate as well. This flaw is evaluated to determine how much effect it has on the results. An additional study is performed to investigate the influence knots in the 0° veneers compared to the 90° veneers. As noted previously the 0° veneers mainly governs the output, therefore a similar Monte Carlo simulation to the previous study is performed with the only difference being that the 90° veneers are considered knot free. The resulting mean and standard deviation of the maximum relative stress distributions for all four layups are compared in Table 5.1 and 5.2.

Table 5.1: Mean for the maximum relative stress distributions.

Case for 90° veneers	Layup 1	Layup 2	Layup 3	Layup 4
Strips	1.60	1.51	1.46	1.46
Knot free	1.60	1.50	1.45	1.45

Table 5.2: Standard deviation for the maximum relative stress distributions.

Case for 90° veneers	Layup 1	Layup 2	Layup 3	Layup 4
Strips	0.170	0.118	0.082	0.073
Knot free	0.168	0.115	0.083	0.070

As seen in the tables above the influence of knots in the 90° veneers make no significant change to either the mean or the standard deviation, for the distributions of the maximum relative stress for any of the studied layups. Based on these results it is assumed that the flaw in the model has a negligible effect on the results. Note that this assumption is restricted to the modeled unidirectional tensile load, meaning it cannot be applied to other load cases such as shear or bending.

6 Conclusions

It is concluded that using the method of back calculating the veneer properties from the data sources of Metsä wood or Tlustochowicz is not an appropriate method. However, it is not ruled out that laminate theory will be able to adequately capture the material behaviour based on other data sources or if additional assumptions are made. For example include the influence of knots and lamination.

The Veneer effect simulations show that the highest relative stress and its variability is lower for thinner layups. It is therefore concluded that for the studied geometry and load case, a thicker layup has a lower yield load compared to a thinner layup.

From the homogenization simulation a wider range of values and higher relative stress are observed in the thinner layups compared to the thicker ones. This is an indication that a homogenization effect is present as the number of veneers increase. Thus it is concluded that the relative stress is less variable and lower for the thicker layups, indicating that sufficiently large structural members can achieve an increased strength due to size because of homogenization. Relating this to Modvion's structure it cannot be stated that the thick LVL will posses a beneficial behaviour with regard to what has been studied in this work. This is due to the veneer effect showing unfavourable response and the homogenization shows favourable effects. The impact of both effects combined will have to be studied in order to establish if a thicker laminate provides a favourable effect or not.

From the distribution of individual knots in the strips, it is observed that the knot pattern highly influences the maximum relative stress. It is concluded that jammed distributions, where two knots are located at a small distance from each other is most critical. In addition one large knot consisting of two or three knots adjacent to each other is not as critical as if they were separated the small distance of 50 mm.

6.1 Future work

In this work the elastic behaviour of the LVL material has been studied, which is a first step in reaching a material model able to determine the strength of the wind turbine tower. The results provide knowledge indicating which research direction to proceed with in order to reach a better understanding of the material. Some of the demarcations made are required to be studied further. The following bullet points propose topics for continued research.

- Timber has some ability to redistribute stresses when loaded above the yield limit. If the yield stress is reached locally, this does not mean the laminate will fail as a component. The 3D material model is linear elastic and therefore plastic redistribution cannot be captured. As a consequence, an elasto-plastic model is desired.
- This work focused on laminates without curvature, loaded in tension with a layup pattern of alternated 0° and 90° veneers. The sequence was chosen to compare the different layups such that the only variable was the number of veneers. As a consequence there is a need to further study alternative layup patterns, different load cases as well as the curvature of the laminates.
- Interfaces between veneers consists of a zone containing a mixture between wood fibers and glue. This can effect the material behaviour between veneers and consequently the performance of the whole laminate.
- The knots in each veneer are in reality shaped like sections of a cone. Also, the fibers are not perfectly aligned, they are distributed organically and the angle from the coordinate axes can differ. In addition there are local fiber deviations around each knot, meaning they also impact the nearby material.
- If there would be no knots in the cross section the maximum relative stress would be significantly lower compared to a case including knots of any distribution. Furthermore, some knot patterns provide higher stress concentrations than others. This gives incentive to investigate further how different production methods can intentionally remove or distribute knots. Potentially reducing or eliminating the increased stress induced from defects.

References

[1] (2020, Mar.) Modvion.
URL: `http://www.modvion.com`

[2] (2020, Mar.) Svenskt Trä.
URL: `https://www.traguiden.se/om-tra/miljo`

[3] *Design of timber structures Volume 1*, 2nd ed., Swedish Forest Industries Federation & Swedish wood, 2016.

[4] *LVL Handbook Europe*, Finnish Woodworking Industries, 2019.

[5] (2020, Feb.) Moelven.
URL: `https://www.moelven.com/se/se/limtra-massivtra-och-lvl/lvl-skivor`

[6] Tomppo, L."Novel Applications of Electrical Impedance and Ultrasound Methods for Wood Quality Assessment," Ph.D. dissertation, University of Eastern Finland, Kuopio Finland, 2013.

[7] *JCSS Probabilistic Model Code, Part 3: Resistance Models*, Joint Committee on Structural Safety, 2006.

[8] Wei, P., Wang, B. J., Wan, X., Chen, X."Modeling and prediction of modulus of elasticity of laminated veneer lumber based on laminated plate theory," *Construction and Building Materials*, vol. 196, pp. 437–442, 2019.

[9] (2020, Feb.) Woodproducts.
URL: `https://www.woodproducts.fi/content/adhesives-wood-construction`

[10] (2020, Jun.) Metsä Wood.
URL: `https://www.metsawood.com/global/Products/kerto/Pages/Kerto.aspx`

[11] Pedersen, M. U., Clorius, C. O., Damkilde, L., Hoffmeyer, P."A simple size effect model for tension perpendicular to the grain," *Wood Sci Technol*, vol. 37, pp. 125–140, 2003.

[12] Blass, H. J., Aune, P., Choo, B. S., Görlacher, R., Griffiths, D. R., Hilson, B. O., Racher, P., Steck, G., Eds.*Timber Engineering STEP 1*. The Netherlands: Centrum Hout, 1995.

[13] *Eurocode 5: Design of timber structures - Part 1-1: General - Common rules and rules for buildings*, CEN European Standard, 2004.

[14] Lukacevic, M., Kandler, G., Hu, M., Olsson, A., Füssl, J."A 3D model of knots and related fiber deviations in sawn timber for prediction of mechanical properties of boards," *Materials and Design*, vol. 166, 2019.

[15] Lang, R., Kaliske, M."Description of inhomogeneities in wooden structures: modelling of branches," *Wood Sci Technol*, vol. 47, pp. 1051–1070, 2013.

[16] Agarwal, B. D., Broutman, L. J., Chandrashekhara, K.*Analysis and performance of fiber composites*, 3rd ed. Wiley, 2015.

[17] Jones, R. M.*Mechanics of composite materials*, 2nd ed. Taylor & Francis, 1999.

[18] "Declaration of Performance - NO. MW/LVL/312-001/CPR/DOP," Metsä Wood, Lohja, Finland.

[19] Tlustochowicz, G."Stabilising System for Multi-Storey Beam and Post Timber Buildings," Ph.D. dissertation, Luleå University of Technology, Luleå Sweden, 2011.

[20] Kohlhauser, C., Hellmich, C."Determination of Poisson's ratios in isotropic, transversely isotropic, and orthotropic materials by means of combined ultrasonic-mechanical testing of normal stiffnesses: Application to metals and wood," *European Journal of Mechanics A/Solids*, vol. 33, pp. 82–98, 2012.

[21] Lukacevic, M., Füssl, J."Numerical simulation tool for wooden boards with a physically based approach to identify structural failure," *European Journal of Wood and Wood Products*, vol. 72, pp. 497–508, 2014.

[22] Fink, G."Influence of Varying Material Properties on the Load-Bearing Capacity of Glued Laminated Timber," Ph.D. dissertation, Graz University of Technology, Zurich Austria, 2014.